Scanning Microscopy

Volume 8 | Number 2 Article 10

7-6-1994

Scanning Electron Microscopy and Energy-Dispersive X-Ray Microanalysis Studies of Several Human Calculi Containing Calcium Phosphate Crystals

Tetsuo Kodaka
Showa University, Japan

Kazuhiro Debari
Showa University, Japan

Tsuneyoshi Sano
Showa University, Japan

Masayuki Yamada
Showa University, Japan

Scanning Microscopy, Vol. 8, No. 2, 1994 (Pages 241-257) 0891-7035/94$5.00+.25
Scanning Microscopy International, Chicago (AMF O'Hare), IL 60666 USA

SCANNING ELECTRON MICROSCOPY AND ENERGY-DISPERSIVE X-RAY MICROANALYSIS STUDIES OF SEVERAL HUMAN CALCULI CONTAINING CALCIUM PHOSPHATE CRYSTALS

Tetsuo Kodaka*, Kazuhiro Debari[1], Tsuneyoshi Sano[2] and Masayuki Yamada

Second and [2]First Departments of Oral Anatomy, School of Dentistry; and [1]EM-Laboratory, Showa University, Tokyo 142, Japan

(Received for publication February 21, 1994 and in revised form July 6, 1994)

Abstract

Human calcium phosphate calculi: two sialoliths, a urolith, a rhinolith, and a tonsillolith were investigated by scanning electron microscopy (SEM) and energy-dispersive X-ray analysis (EDX). The sialoliths and urolith had appositional shells with thick cortices, respectively, around several nuclei composed of calcospherulites and a rubber-film fragment. The rhinolith had a thin cortex with appositional laminations around a glomerulus-like mass of calcified cotton-like strings. The tonsillolith had a rough cortex with appositional laminations. Its porous interior was composed of numerous calcified conglomerates with microorganisms and calcified masses with fine appositional laminations around the conglomerates. The major crystals were identified as biological apatites (AP) with a sand-grain rather than a needle-like shape, and plate-shaped octacalcium phosphate (OCP). The AP deposits of the rhinolith probably were associated with magnesium (Mg) phosphates or contained Mg. No OCP was found in the rhinolith. The AP deposits were mainly formed by extracellular calcification. Hexahedral crystals, identified as Mg-containing whitlockite (WH), were precipitated in the internal spaces of the AP and OCP deposits. The rhinolith nucleus consisted of WH crystal deposits only.

Key Words: Scanning electron microscopy, backscattered electron imaging, energy-dispersive X-ray microanalysis, sialolith, urolith, rhinolith, tonsillolith, calcium phosphates, crystal habits, formation.

*Address for Correspondence:
Tetsuo Kodaka,
Second Department of Oral Anatomy,
School of Dentistry, Showa University,
1-5-8 Hatanodai, Shinagawa-ku,
Tokyo 142, Japan
Telephone number: (81)-3-3784 8157
FAX number: (81)-3-3786 0072

Introduction

Among human calcium phosphate calculi or stones, there exist dental calculus [19, 26, 28, 32, 33, 35, 45, 52-55, 57, 60, 66, 71, 80, 81, 84-86, 88], sialoliths or salivary stones [3, 7, 10, 19, 24, 25, 31, 42, 60, 69, 82], and uroliths including renal [16, 74] and urinary stones [15, 27, 39, 42-44, 58, 67, 78, 83, 89, 94]. In addition, rhinoliths or nasal stones [1, 4, 15, 75, 76], tonsilloliths or tonsillar stones [12, 17, 21], pancreatic calculus [78], uterine stones [15, 39, 40], gallstones [36, 95], and other stones [42, 50] are also known.

In calcium phosphate crystals of these stones, there exist biological apatites (AP) including Ca-deficient and carbonate apatites [3, 7, 10, 15, 17, 19, 23, 39-45, 48, 50, 57, 58, 60, 66, 69, 78, 82, 83, 89, 94] or hydroxyapatite (HAP) [$Ca_{10}(PO_4)_6(OH)_2$; 1, 16, 17, 26, 28, 31, 32, 35, 41, 42, 55, 71, 80, 81, 85-88, 89], brushite or dicalcium phosphate dihydrate (DCPD) [$CaHPO_4$-$2H_2O$; 10, 16, 19, 28, 35, 39, 42-44, 57, 60, 66, 76, 78-80, 82, 85, 86, 88, 89], octacalcium phosphate (OCP) [$Ca_8(PO_4)_4(HPO_4)_2$-$5H_2O$; 10, 19, 28, 35, 42, 48, 54, 55, 57, 60, 66, 80, 84-86, 88, 89], and β-tricalcium phosphate or whitlockite (WH) [$Ca_{10}(HPO_4)(PO_4)_6$; 3, 7, 10, 19, 28, 31, 32, 35, 42, 43, 69, 80, 82, 83, 85, 86, 88, 89]. The WH crystals of dental calculus usually contain magnesium and they are called Mg-substrate or Mg-containing WH [$Ca_9Mg(HPO_4)(PO_4)_6$; 19, 29, 45, 48, 52, 53, 55, 60, 66, 71].

From the chemical formulas given above, the ideal Ca/P molar ratios for different calcium phosphate crystals are as follows; 1.67 for HAP (less than 1.67 for AP), 1.00 for DCPD, 1.33 for OCP, and 1.50 for WH; while the Ca/P molar ratio of Mg-containing WH ranges from 1.29 to 1.43 [11, 19, 25, 38].

Their native and synthetic crystal habits are as follows; HAP and AP are hexagonal dipyramidal, needle, and rod-like in shape [9, 19, 22, 26, 37, 44, 48, 57, 60, 62, 70-72, 81, 83, 85, 87, 90]; DCPD is a triangular plate, polygonal column, and rhombohedral in shape [5, 6, 15, 19, 44, 57, 60, 64-66, 70, 78, 79, 85]; and OCP is ribbon, flake, and plate-like in shape [9, 13,

19, 48, 54, 55, 57, 59, 60, 62, 63, 66, 70, 72, 84]; WH and Mg-containing WH are rhombohedral and cuboidal (hexahedrally based) in shape [11, 18, 19, 25, 38, 48, 52, 53, 55, 56, 60, 61, 66, 71, 72, 83]. On the other hand, the fine crystals of AP under scanning electron microscopy (SEM) may show a sand-grain rather than a needle-like shape [48, 50, 51, 55, 57], because the surfaces, usually, must be coated with a thin metal layer in order to prevent electrostatic charging during the observations.

Such crystal shapes and Ca/P molar ratios can be used as indicators of biological calcium phosphate crystals as reported in dental calculus [48, 52-55, 58, 66, 71]. In this study, the structure and calcified components of several human stones and their calcium phosphate crystals were investigated by SEM, including the secondary electron (SE) and the backscattered electron (BSE) signals, and energy-dispersive X-ray (EDX) microanalysis. Thus, the crystal compositions and fine structure were compared with those of previous studies; in addition, the formation patterns were discussed since their distribution patterns were observed.

Materials and Methods

Large and smaller sialoliths (about 7 x 8 x 14 mm and 3 x 4 x 9 mm in size) were removed from the parotid gland duct of a female aged 34 years or, respectively, from the submandibular gland duct of a female aged 32 years. A large oval-shaped urolith (about 18 g in dry weight, 19 x 26 x 34 mm in size) was collected from the urinary bladder of a male aged 66 years. A rhinolith (about 1 g, 8 x 13 x 19 mm) was obtained from the inferior nasal meatus of a female aged 23 years and a tonsillolith (about 0.8 g, 8 x 10 x 22 mm) from the palatine tonsil of a female aged 56 years.

These stones (two sialoliths, an urolith, a rhinolith, and a tonsillolith: Figs. 1a-4a) were fixed in 10% neutral formaldehyde for a few days and then preserved in 70% ethanol. After rinsing in running water and drying in the air, they were cut into several slices with a diamond wheel or fractured into several pieces with a bone chisel and a hammer. One slice or piece of each stone was embedded in epoxy resin (Epo-Mix Epoxide; Buehler, U.S.A.). The resin-embedded samples were ground with grinding stones and polished with 5 and 0.3 μm alumina on polishing cloths. For observation of calcified structures [8, 34, 36, 49, 51], the composite images by the BSE were photographed with a Hitachi S-2500CX SEM operated at an accelerating voltage of 25 kV and a specimen irradiation current of 5 x 10^{-6} mA, after carbon coating in a high vacuum evaporator (HUS-5GB; Hitachi, Japan).

The samples of the sialoliths and tonsillolith were polished again in order to remove a carbon membrane, and the exposed surfaces were treated with about 10% sodium hypochlorite (NaOCl) for 30 minutes and then 2% ethylenediamine tetra-acetic acid (EDTA) at pH 7.2 for 1 minute; this combined treatment of NaOCl and EDTA was repeated 3 times in order to make a strong relief. Such a method has been useful for SEM observations of laminar and globular calcified deposition in human dentin [46], and appositional laminations and nuclei in human pineal calcareous concretions [50]. This was followed by rinsing in running water, drying in the air, and coating with a 10-15 nm thick platinum-palladium (Pt-Pd) layer in an ion sputtering apparatus (IB-5; Eiko, Japan). The SE images were observed with a Hitachi S-430 SEM at 20 kV. We call this the NaOCl-EDTA/SEM method.

The remaining untreated samples were fractured into several small pieces. About half of them were coated with carbon so that the principal elements of Ca, P, and Mg in a mass which involved much the same crystals in shape and size were quantitatively analyzed at 10 points using a Hitachi X-560 SEM fitted with a Kevex 7000Q EDX detection system at an accelerating voltage of 15 kV, a beam current 1 x 10^{-7} mA, and 150 seconds counting time. The standard samples were native fluorapatite and magnesium oxide. The remaining fractured pieces were treated with about 10% NaOCl for 30 minutes in order to remove organic substances [30, 34, 46, 48, 51-55, 57]. The SE images of all the fractured samples were observed with a Hitachi S-430 SEM after coating with a Pt-Pd layer.

Results

The EDX analysis detected mainly Ca and P with or without traces of Mg from crystal deposits in these stones treated with no NaOCl nor EDTA. Table 1 shows the concentrations of Ca, P, and Mg (percent by weight), and their molar ratios in three types of crystals such as: sand-grain or larger granule, plate, and hexahedron in shape (Figs. 1-4).

Figure 1a shows the entire view of two sialoliths. In the BSE-SEM (Figs. 1b and 1c), the large and smaller stones showed a rhythmical apposition of alternating shells around the several nuclei (Fig. 1b). The hypercalcified shells measured 2-12 μm in thickness and the un- or hypocalcified sites between the shells showed 2-14 μm (Fig. 1c). In the calcified nuclei, numerous calcospherulites measuring 3-5 μm in diameter were clearly exposed with the NaOCl-EDTA/SEM method (Fig. 1d). When observed with the SE-SEM after NaOCl treatment, the shells showed a dense layer of fine sand-grain shaped crystals without microorganisms (Fig. 1e), a relatively loose layer of larger granule-shaped

Table 1. The concentrations of Ca, P, and Mg, and their molar ratios of three crystal types observed in human stones.

Human stone	Crystal type	Percent by weight Ca	P	Mg	Molar ratio Ca/P	Ca+Mg/P	Mg/Ca
Sialoliths	AP	32.27±0.82	17.73±0.23	-	1.44±0.03	-	-
(Fig. 1)	OCP	29.68±0.90	16.72±0.43	-	1.37±0.03	-	-
	WH	27.35±1.07	15.38±0.49	1.06±0.04	1.38±0.04	1.47±0.02	0.06±0.02
Urolith	AP	31.56±0.83	17.25±0.98	1.67±0.50	1.42±0.05	1.54±0.03	0.09±0.02
(Fig. 2)	OCP	29.36±1.66	17.68±2.32	-	1.30±0.15	-	-
	WH	29.36±0.43	19.49±0.69	3.73±0.47	1.18±0.63	1.41±0.01	0.21±0.02
Rhinolith	AP	30.97±0.53	14.47±0.32	-	1.65±0.03	-	-
(Fig. 3)	WH	27.93±0.53	16.27±0.43	1.50±0.23	1.33±0.02	1.45±0.01	0.09±0.01
Tonsillolith	AP	31.25±1.43	16.02±0.86	-	1.51±0.09	-	-
(Fig. 4)	OCP	30.79±0.72	17.32±0.62	-	1.38±0.03	-	-
	WH	27.92±1.86	17.40±0.94	2.72±0.29	1.24±0.02	1.44±0.02	0.16±0.02
Dental calculus*	AP	31.20±0.86	14.78±0.47	-	1.64±0.04	-	-
	OCP	27.86±1.57	16.53±0.77	-	1.30±0.03	-	-
	WH	31.71±0.41	19.19±0.41	1.98±0.13	1.28±0.02	1.42±0.03	0.10±0.01

AP: sand-grain or granule-shaped crystals; OCP: plate-shaped crystals; WH: hexahedral crystals.
*cited from reference [48]. Mean ± standard deviation (n = 10)

crystals with bacterial molds (Fig. 1f), and a layer of plate-shaped crystals arranged vertically to the shells (Fig. 1g). Hexahedral crystals were present between the shells (Fig. 1h).

Figure 2a shows the entire view of an urolith taken from an urinary bladder. The stone consisted of appositional shells with a thick cortex concentrically around the central nucleus consisting of a fragment of a rubber film, visible in the fractured surface with the naked eye (Fig. 2b). The BSE image showed that the shells which were occasionally penetrated by the radial arrangement of plate-shaped crystals were loosely calcified (Fig. 2c), and that the thin calcified shells measured about 20 μm (Fig. 2d). When observed with the SE-SEM after NaOCl treatment, the shells were composed of sand-grain or larger granule-shaped crystals with microorganisms and bacterial molds (Figs. 2e and 2f). The radial arrangement was composed of plate-shaped crystals in various shapes and sizes (Fig. 2g). Hexahedral crystals were found between the shells and with the plate-shaped crystals (Fig. 2h).

Figure 3a shows the entire view of a rhinolith. In the BSE, the calcified cortex measuring 40-250 μm in thickness had appositional laminations of 5-10 μm in periodicity (Fig. 3b). The SE-SEM after NaOCl treatment showed that the cortex was composed of sand-grain-shaped crystals with microorganisms and bacterial molds (Fig. 3c), and that the interior or large nucleus showed a glomerulus-like structure of calcified strings measuring 10-30 μm in diameter (Fig. 3d). The BSE images indicated that the strings showed a tubular structure and a lower calcification than the surrounding deposits in the outer nucleus layer (Fig. 3e). Some of the strings had hypercalcified grains attached to the outer and inner walls of the tubules. In the inner nucleus, the tubular strings were occupied with the grains and some of the grains filled the tubular lumens (Fig. 3f). Among the strings, calcified masses of grain-shaped deposits were scattered. When observed with the SE-SEM, numerous hexahedral crystals were found among the tubular strings (Fig. 3g), and on the outer surfaces (Fig. 3h with inset) and in the lumens (Fig. 3h). Such crystals agreed with

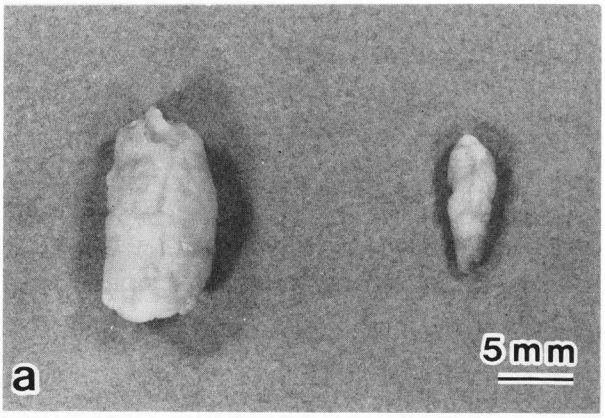

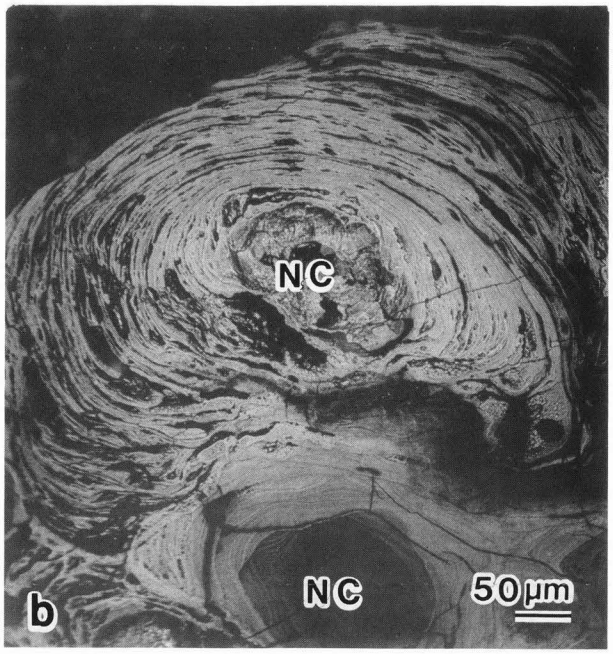

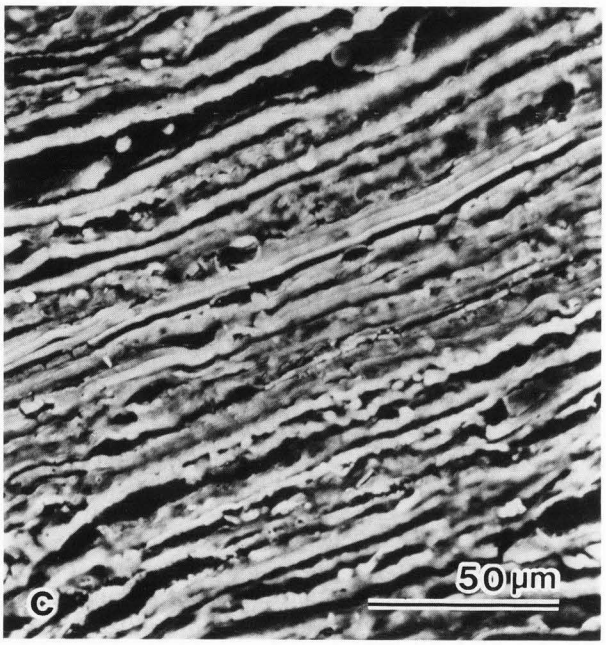

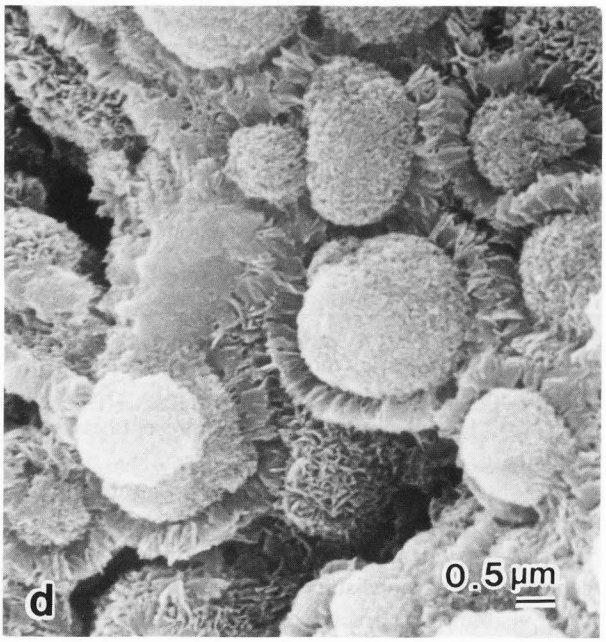

Figure 1 (a-d, above; e-h, on the facing page 245). Sialoliths.

(**a**) A macrophotograph of the entire view of large and smaller stones taken from the parotid gland duct of a middle-aged female and the submandibular gland duct of a middle-aged female.

(**b-d**) The ground surfaces: the BSE images showing the appositional laminations (**b**, **c**) and the SE image with the NaOCl-EDTA/SEM method showing the calcospherulites in one of the nuclei (**d**).

(**e-h, on the facing page**) The SE images of crystals on the fractured surfaces treated with NaOCl: sand-grain-shaped crystals with no microorganisms (**e**) and larger granule-shaped crystals with bacterial molds (**f**), plate-shaped crystals in several shells (**g**), and hexahedral crystals between shells (**h**).

NC = nucleus of the stone. Arrow = bacterial mold.

the grain-shaped deposits observed with the BSE (Figs. 3e and 3f). No plate-shaped crystals could be found in the stone.

Figure 4a shows the entire view of a tonsillolith. The BSE image indicated that the rough cortex had many calcified projections with poor appositional laminations in the outermost layer (Fig. 4b). The cortex thickness ranged from 20 to 200 μm. Under the SE-SEM images, the porous interior was divided into two different structures; calcified masses connected with each other (Fig. 4c), and roughly aggregated structures of a

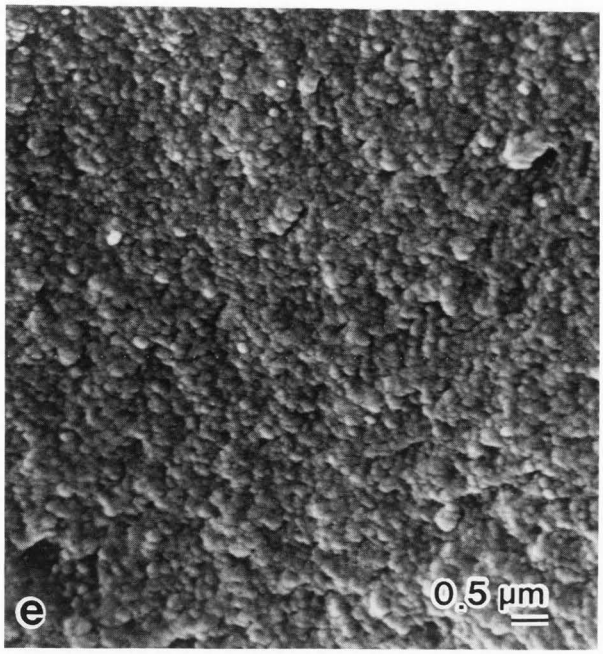

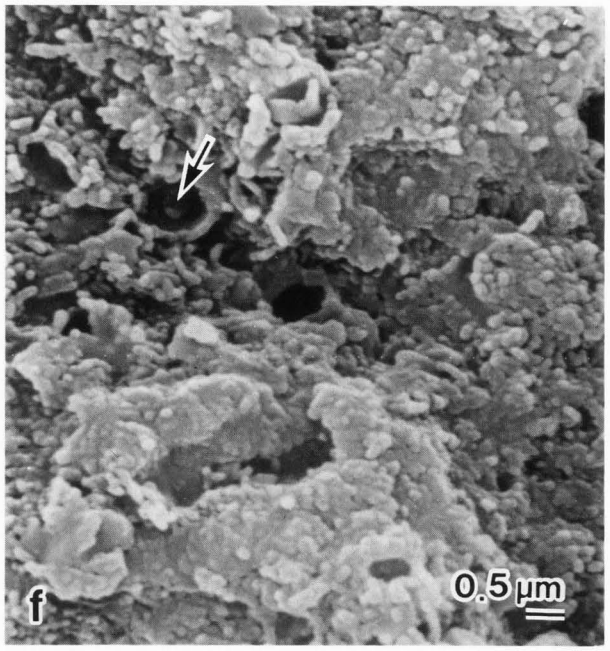

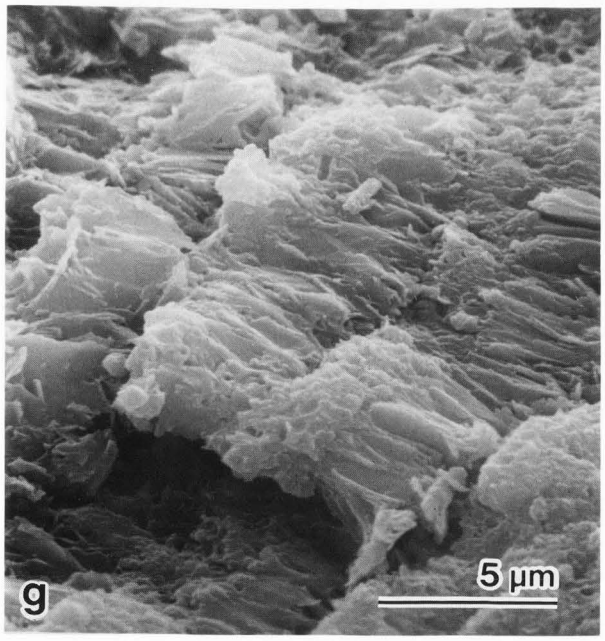

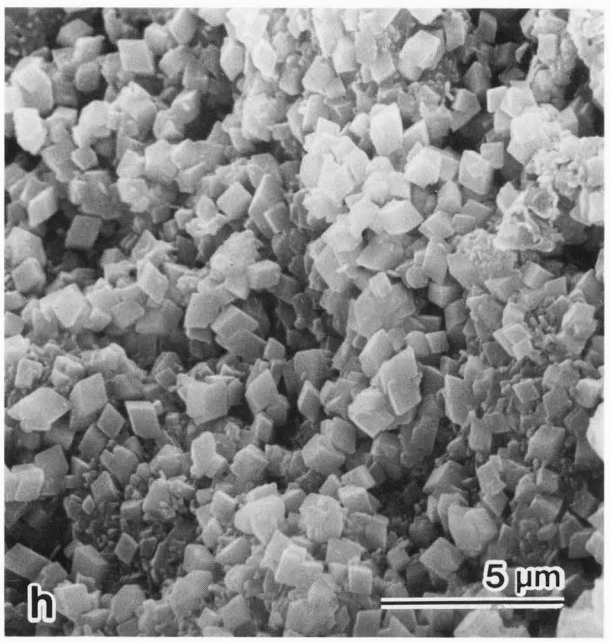

large number of calcified conglomerate bodies measuring 5-20 μm in diameter (Fig. 4d). In the masses, the conglomerates were occasionally embedded and the appositional laminations were concentrically arranged around the conglomerates as nuclei in the BSE (Fig. 4e). The appositional laminations showed intervals of 2-9 μm in the BSE, but the minimum intervals were about 0.5 μm in the NaOCl-EDTA/SEM method (Fig. 4f). The aggregated conglomerates were loosely and concentrically arranged as seen in the BSE image (Fig. 4g), and the larger conglomerates showed a few concentric laminations (Fig. 4g inset). In the SE-SEM with non-treatment (Fig. 4h) and in the NaOCl-EDTA/SEM method (Fig. 4i), microorganisms and bacterial molds were observed on and in the conglomerates, respectively. The cortex and interior were mainly composed of sand-grain-shaped crystals with bacterial molds (Fig. 4j). In some parts of the cortex, elongated plate-shaped crystals were arranged vertically to the natural surface (Fig. 4k). Hexahedral crystals were observed in the intra-spaces of the stone (Fig. 4l).

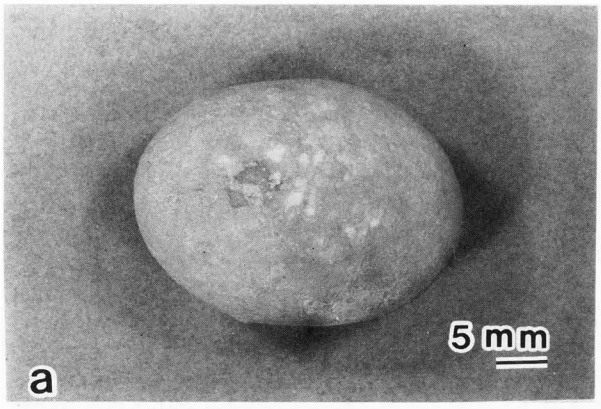

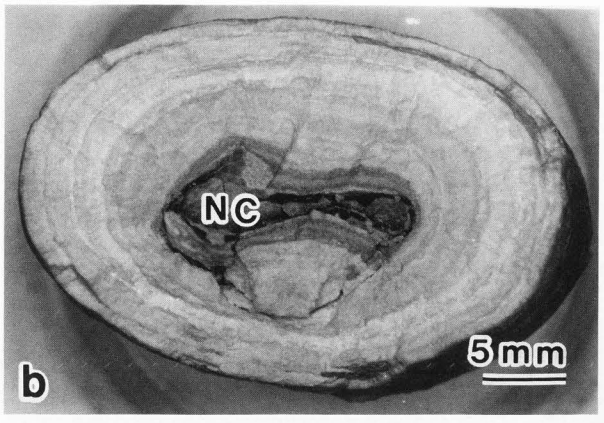

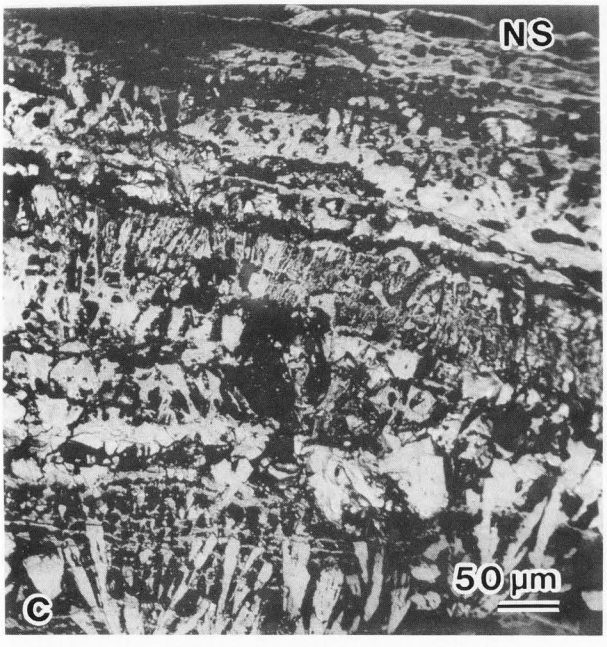

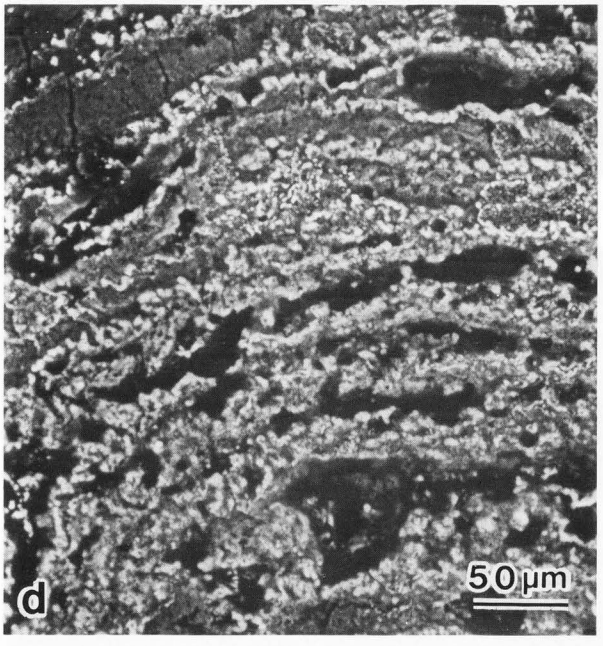

Table 2. The concentrations of Ca and P, and the molar ratio of the sialolith and tonsillolith nuclei (mean ± standard deviation; n = 5). These basic structures are shown in Figure 1d, and Figures 4d and 4g-4i, respectively.

Calcified structures	Percent by weight Ca	P	Molar ratio Ca/P
Spherulites (Sialolith)	31.57 ±0.05	14.90 ±0.37	1.64 ±0.03
Glomerates (Tonsillolith)	33.78 ±0.52	16.22 ±0.69	1.61 ±0.07

Figure 2 (a-d, above; e-h, on the facing page 247). Urolith: taken from the urinary bladder of an old male. NS = natural surface of the stone.

(**a**, **b**) Macrophotographs of the entire view (**a**) and the fractured surface (**b**): concentric shells are seen around a nucleus (NC) where a rubber fragment was found.

(**c**, **d**) The BSE images of the ground surface.

(**e-h, on the facing page**) The SE-SEM images of the fractured surfaces treated with NaOCl: sand-grain (**e**) and larger granule-shaped crystals (**f**) with micro-organisms (double arrows) and bacterial molds (arrow), plate-shaped crystals (**g**), and hexahedral crystals between shells (**h**).

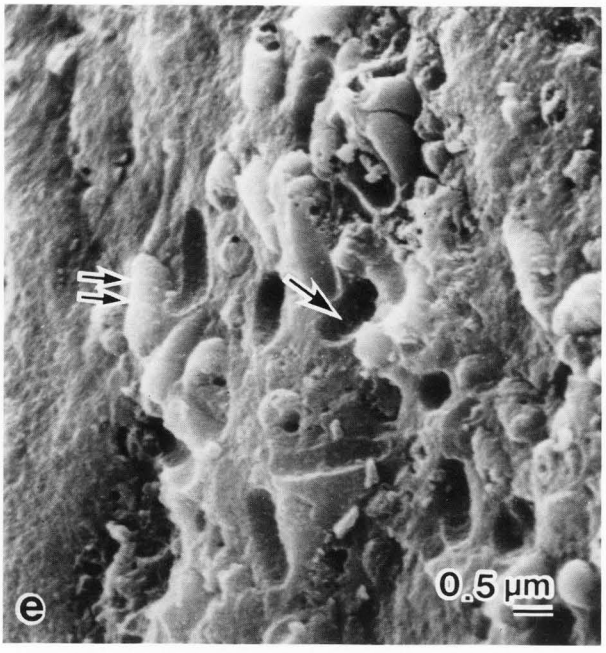

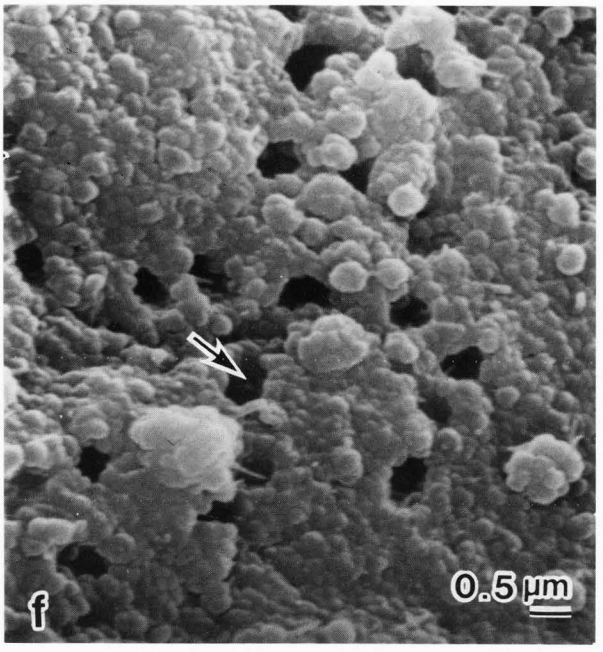

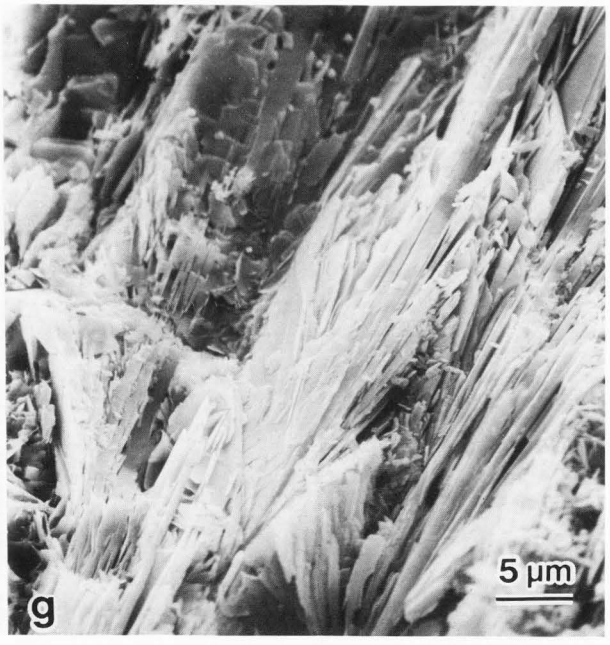

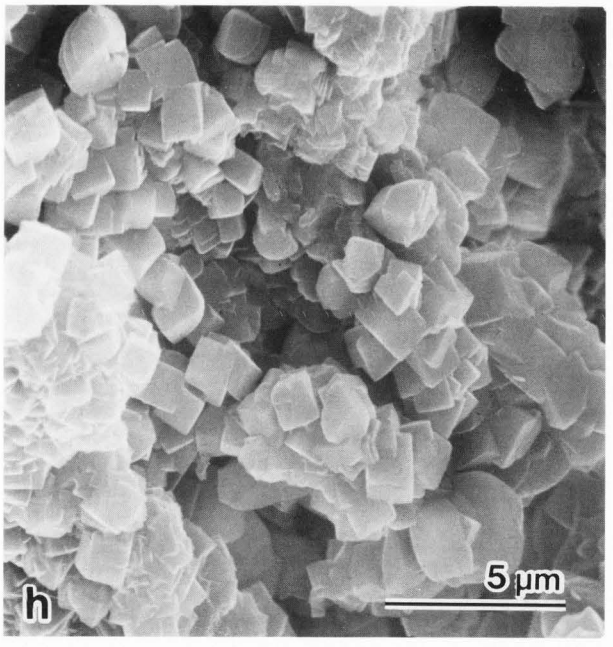

Table 1 shows, that the sand-grain and larger granule-shaped crystal deposits in the sialoliths (Figs. 1e and 1f), rhinolith (Figs. 3b and 3c), and tonsillolith (Fig. 4j) showed a Ca/P molar ratio ranging from 1.44 to 1.65, while the urolith crystal deposits (Figs. 2e and 2f) contained low Mg and the Ca/P molar ratio was 1.42. The plate-shaped crystals (Figs. 1g, 2g, and 4k) showed a Ca/P molar ratio ranging from 1.30 to 1.38. The hexahedral crystals (Figs. 1h, 2h, 3g, and 4l) always contained low Mg as well as high Ca and P. The Ca/P, (Ca+Mg)/P, and Mg/Ca molar ratios were, respectively, 1.18-1.38, 1.41-1.47, and 0.06-0.21. The nuclei of the sialolith spherulites (Fig. 1d) and the tonsillolith conglomerates (Figs. 4d, 4g-4i), in which high Ca and P but no Mg was detected, showed Ca/P molar ratios of 1.64 and 1.61, respectively (Table 2).

Discussion

Sialoliths [2, 3, 7, 23, 42, 69] and large uroliths [39, 42, 44, 67] show concentric shells with alternating zones of hyper- and non- or hypocalcifications around

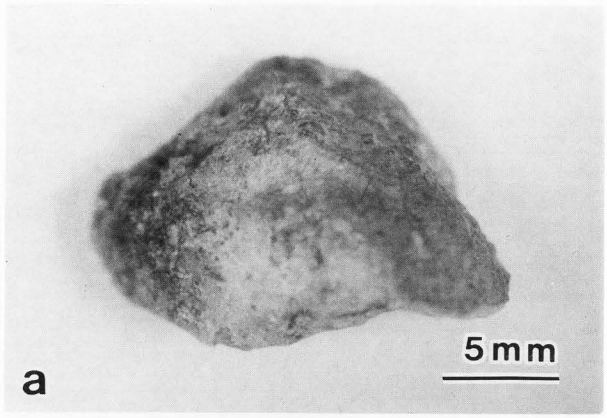

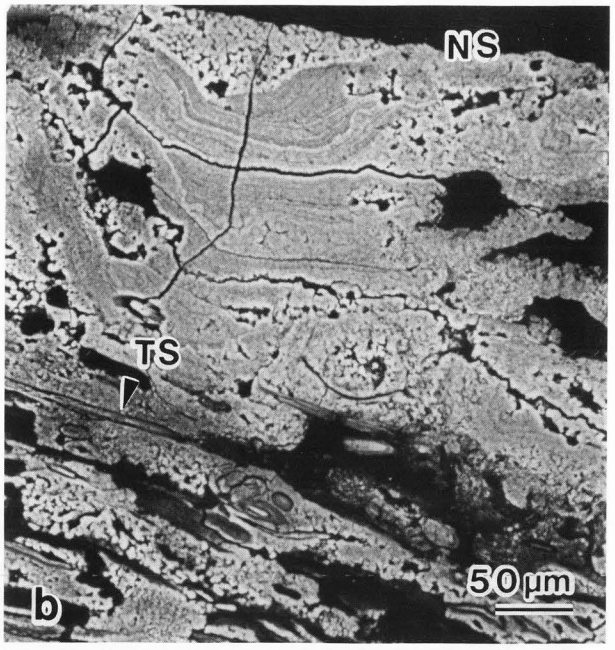

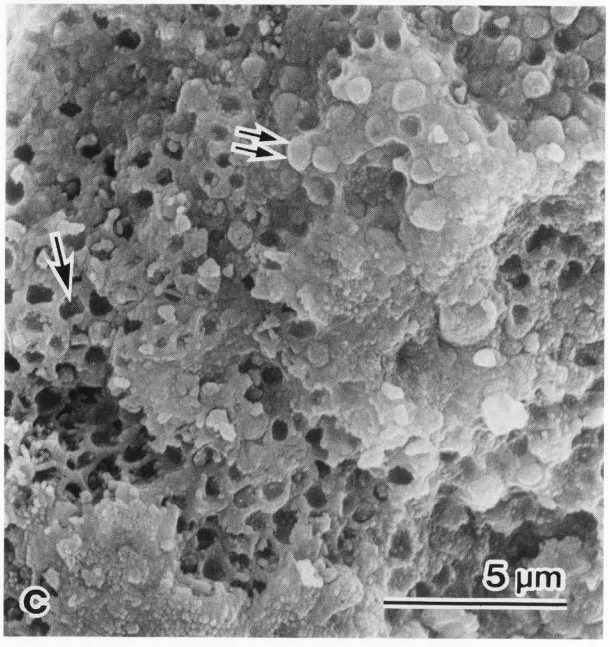

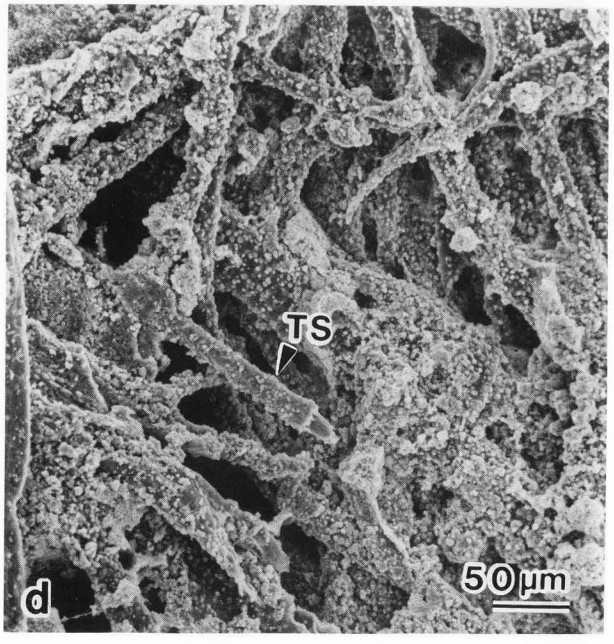

Figure 3 (a-d, above; e-h on the facing page 249). Rhinolith: taken from the inferior nasal meatus of a young female.

(**a**) A macrophotograph of the entire view.

(**b**, **c**) The cortex: the BSE image of the ground surface (**b**) and the SE-SEM image of the fractured surface treated with NaOCl showing sand-grain-shaped crystals (**c**).

(**d-h**; **e-h on the facing page**) = The interior: the SE images after NaOCl treatment of the central nucleus (**d**), the BSE images of the outer nucleus layer (**e**) and the central nucleus (**f**), and the SE images of hexahedral crystals (WH) among the tubular strings (**g**) and on (**h**, **h inset**) and in them (**h**).

NS = natural surface of the stone. Arrow = bacterial mold. Double arrows = microorganism. TS = tubular string. TL = tubular lumen. OS = outer surface of a string. For Figure 3h inset, bar = 0.5 μm.

their nuclei similar to a large uterine stone [41]. The sialoliths and urolith in this study were formed by rhythmical deposition of minerals around their nuclei (Figs. 1b; 2b, and 2c) as reported previously. However, we revealed, using BSE imaging (Figs. 1c and 2d) that the shells were thin compared with those in previous studies. The calcified nuclei of the sialoliths contained many calcospherulites (Fig. 1d), although the initial materials, which may be of native origin [2, 7], could not be identified. The urolith nucleus was a rubber film. It may be a fragment of a catheter, which is one

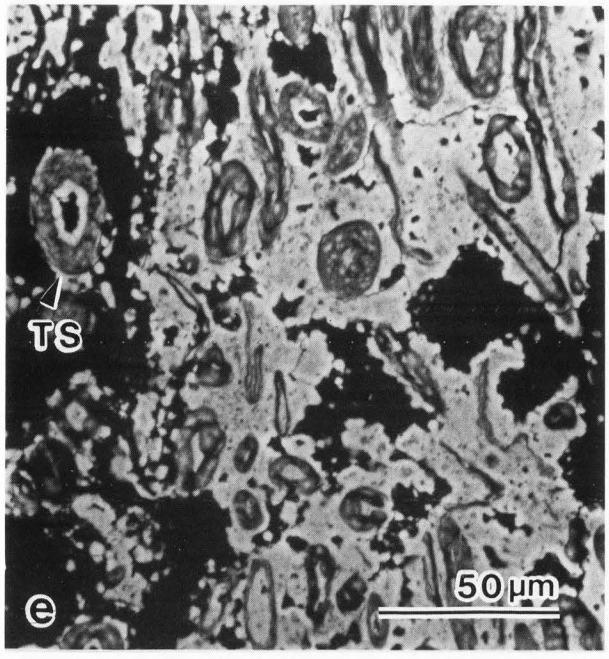

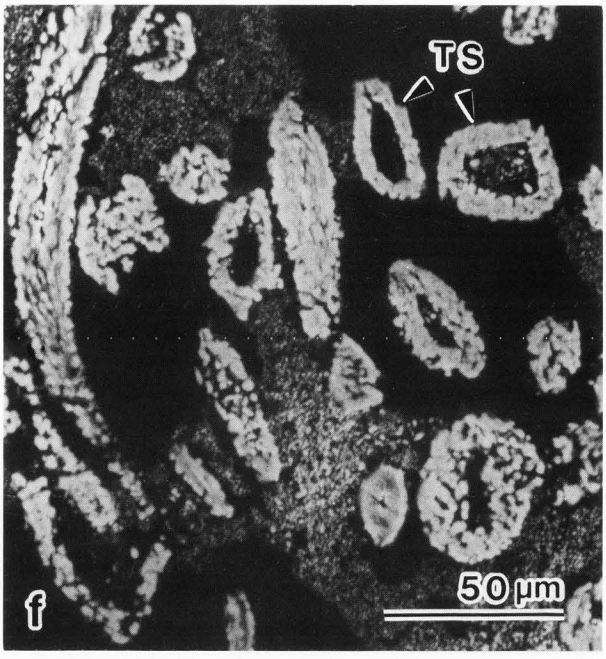

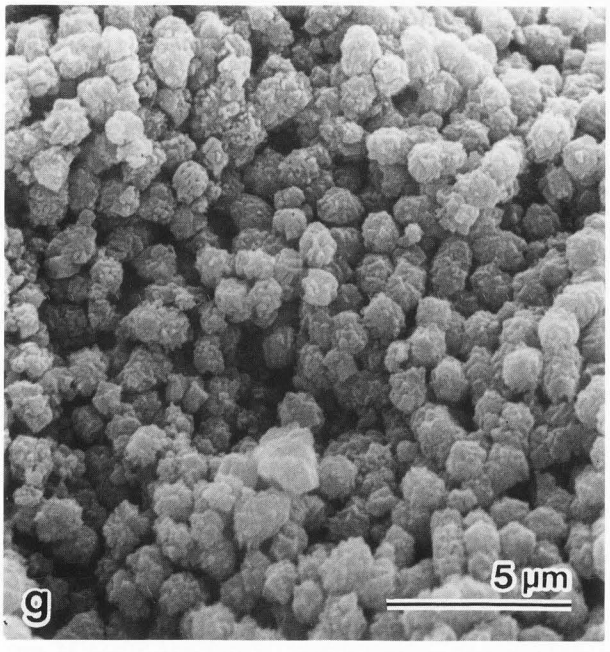

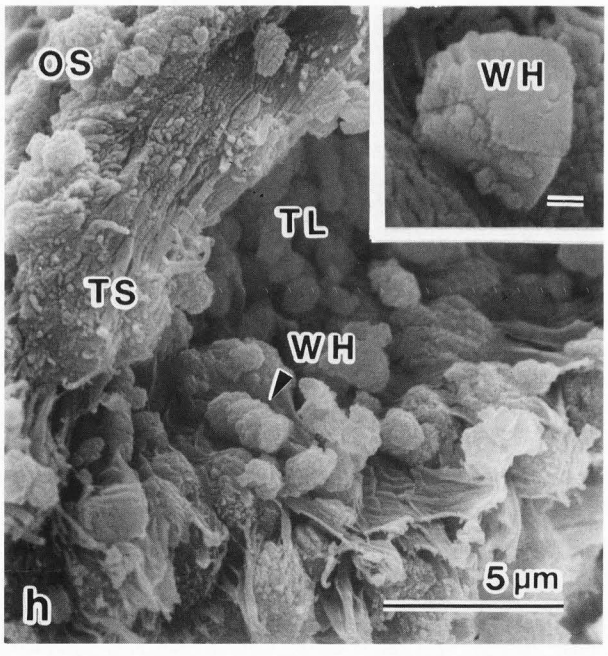

of the possible foreign nuclei other than intrauterine contraceptive devises, suture materials, and surgical staple fibers [15, 40, 41].

In rhinoliths and tonsilloliths, no rhythmical deposition of minerals has been reported. However, we found appositional laminations in their thin cortices (Figs. 3c and 4b); in addition, the tonsillolith also showed fine laminated structures in its interior (Figs. 4e and 4f). In the rhinolith, the large glomerulus-shaped nucleus of the calcified tubular strings (Figs. 3d-3f) is probably cotton strings crumpled into a ball; pressed paper [76], a nut [15], and a pink bead [4] have previously been reported as foreign nuclei. The calcified nuclei of the tonsillolith are probably numerous conglomerates with microorganisms (Figs. 4h and 4j); however, the initial materials which may be of native origin [17, 68] could not be identified in this study. The formation patterns of these stones will be discussed in the last paragraphs of this **Discussion**.

As noted in the **Introduction**, fine crystals of biological apatites under the SE-SEM were generally sand-grain-shaped rather than needle-shaped [48, 50, 51, 55,

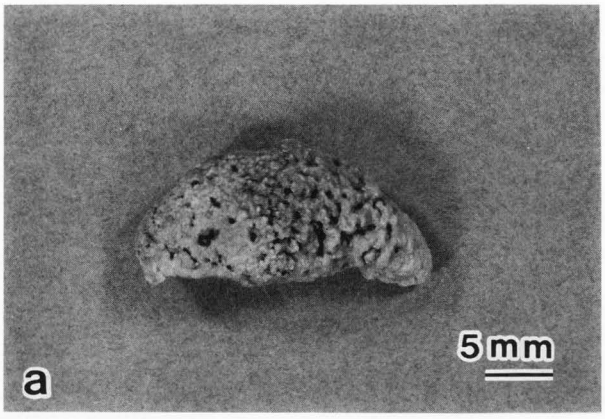

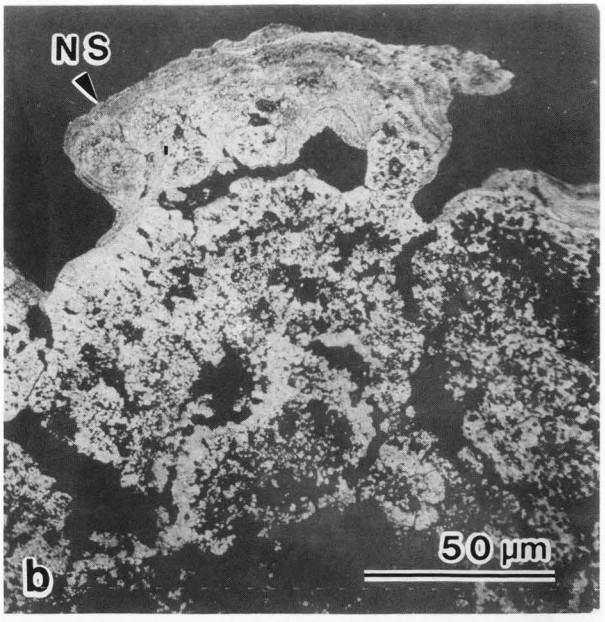

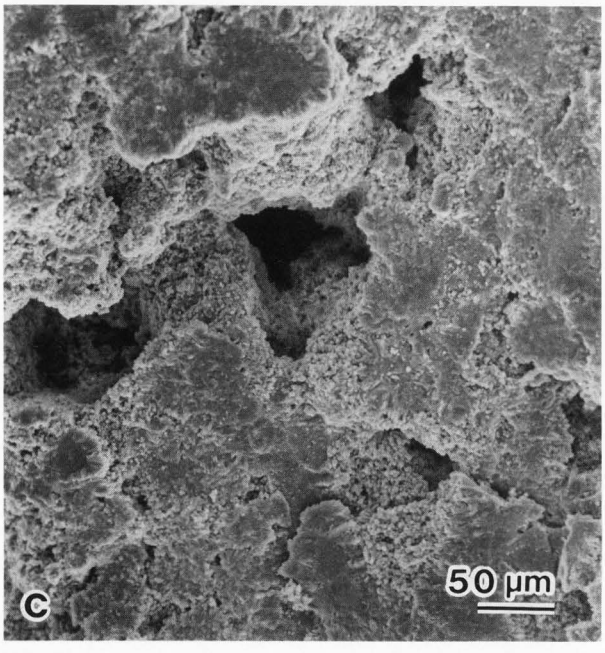

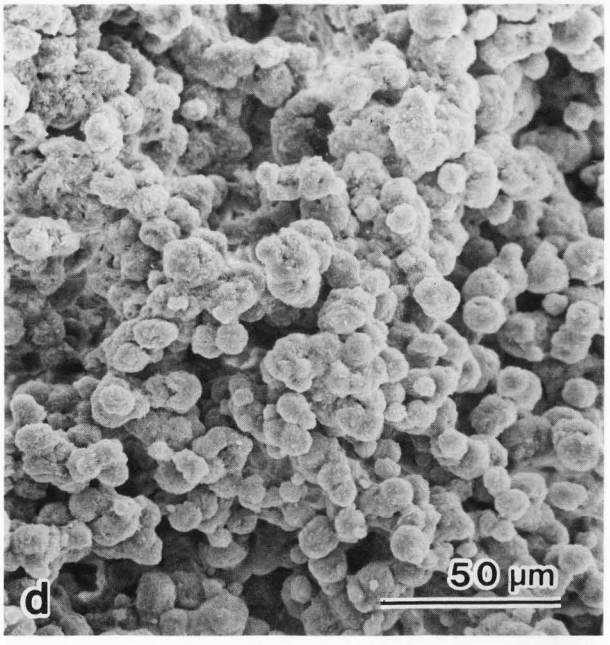

Figure 4 (a-d above, e-h on page 251, and i-l on page 252). Tonsillolith: taken from the palatine tonsil of an o]d female. (**a**) A macrophotograph of the entire view. (**b**) The BSE image of the ground surface: the rough cortex with the porous interior. (**c**, **d**) The SE-SEM images of the fractured surfaces treated with NaOCl: the calcified masses (**c**) and the conglomerates in the interior (**d**). (**e**, **f**) The calcified masses with the appositional laminations in the interior: the BSE (**e**) and the SE image with the NaOCl-EDTA/SEM method (**f**). (**g-i**) The conglomerates in the interior: the BSE image (**g**, **g inset**) and the SE images with non-treatment (**h**) and the NaOCl-EDTA/SEM method (**i**). (**j-l**) The SE images after NaOCl (**j**, **l**) and non-treatment (**k**): sand-grain-shaped crystals with bacterial molds (**j**), plate-shaped crystals in the cortex (**k**), and hexahedral crystals (**l**). NS = natural surface of the stone. GB = glomerate body. Arrow = bacterial mold. Double arrows = microorganism. For Figure 4g inset, bar = 5 μm.

57], because the surfaces had been coated with a metal layer before the observations. From our SE-SEM images with a metal-coated layer (Figs. 1-4) and EDX data (Table 1), and a large number of previous studies [1, 3, 5-7, 10, 11, 13, 15-19, 22, 25, 26, 28, 29, 31, 32, 35, 37-45, 48, 50-66, 69-72, 75, 76, 78-90, 94], the sand-grain and larger granule-shaped crystals, except for those in the urolith, were identified as biological apatites (AP) including Ca-deficient or carbonate apatites; while the plate-shaped and the hexahedral crystals, respectively, were identified as octacalcium phosphate (OCP) and Mg-containing whitlockite (WH). The sialolith spherulites and the tonsillolith conglomerates in their nuclei

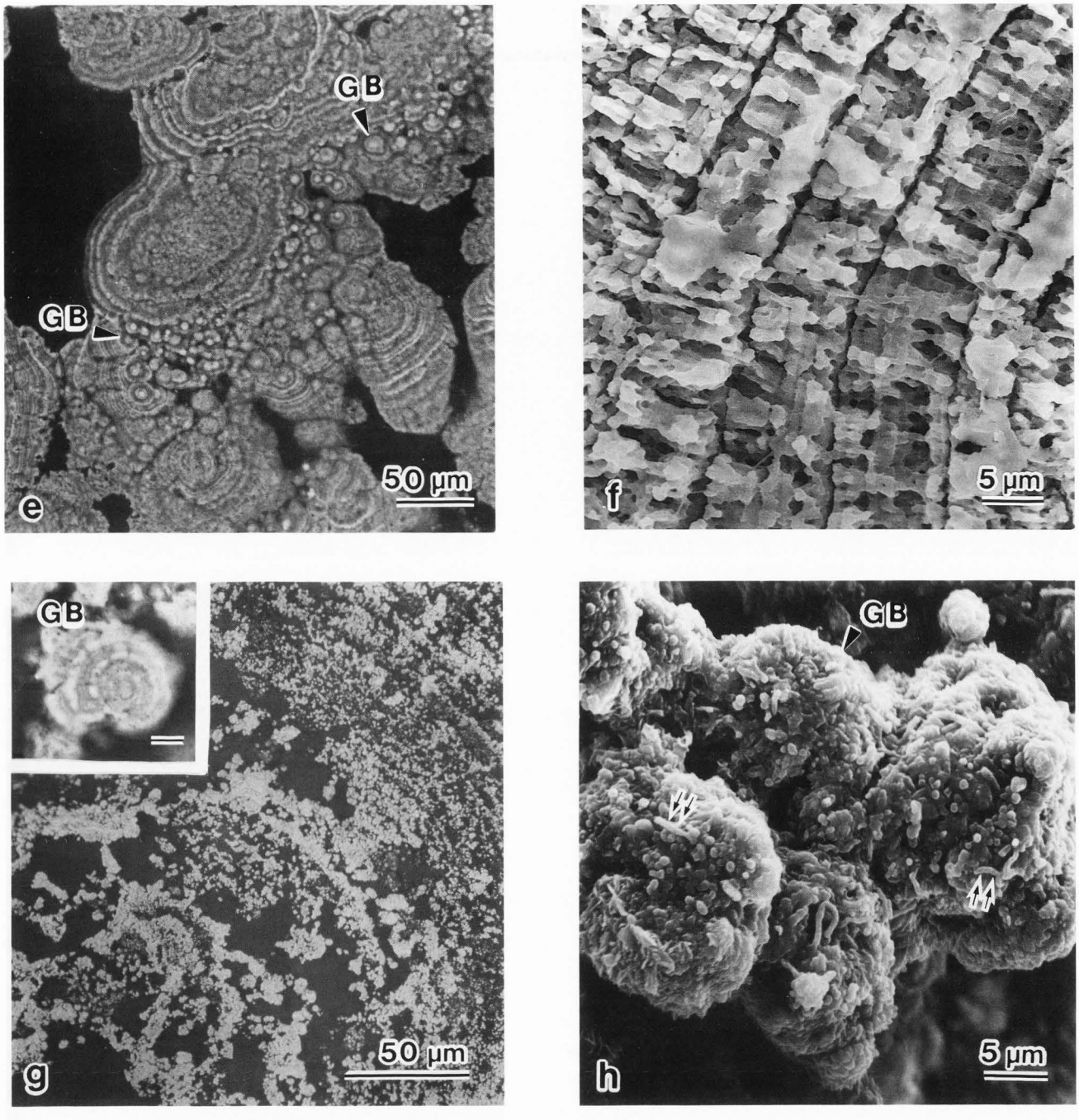

(Figs. 1d; 4d, 4g-4i) were identified as masses of AP from their Ca/P molar ratios (Table 2) and the structures similar to them composed of AP [39, 40, 42, 44, 78].

The sand-grain and larger granule-shaped crystal deposits in the urolith contained low Mg as well as high Ca and P (Figs. 2e and 2f; Table 1). They are probably composed of AP crystals with magnesium phosphates, as reported previously in uroliths [16, 39, 43, 87] or Mg-containing AP [14, 19, 20, 60, 61, 73, 91]; in addition, some magnesium phosphates may include struvite [78, 94]. On the other hand, most of the dense deposits of sand grain-shaped crystals in all the stones used in this study were mainly formed by extracellular calcification with microorganisms (Figs. 1f, 2f, 3c, and 4j) as those in dental calculus [26, 48, 55, 57, 81, 85, 87]; in addition, such crystals have been reported as AP or hydroxyapatite (HAP). The same calcification was also reported in uroliths [42, 67, 83] and in a uterine stone [41].

The calcium phosphate crystals identified in this study were compared with those in previous reports. In sialoliths, AP and WH [3, 7, 31, 69]; and AP, dicalcium phosphate dihydrate (DCPD), and WH [82] were

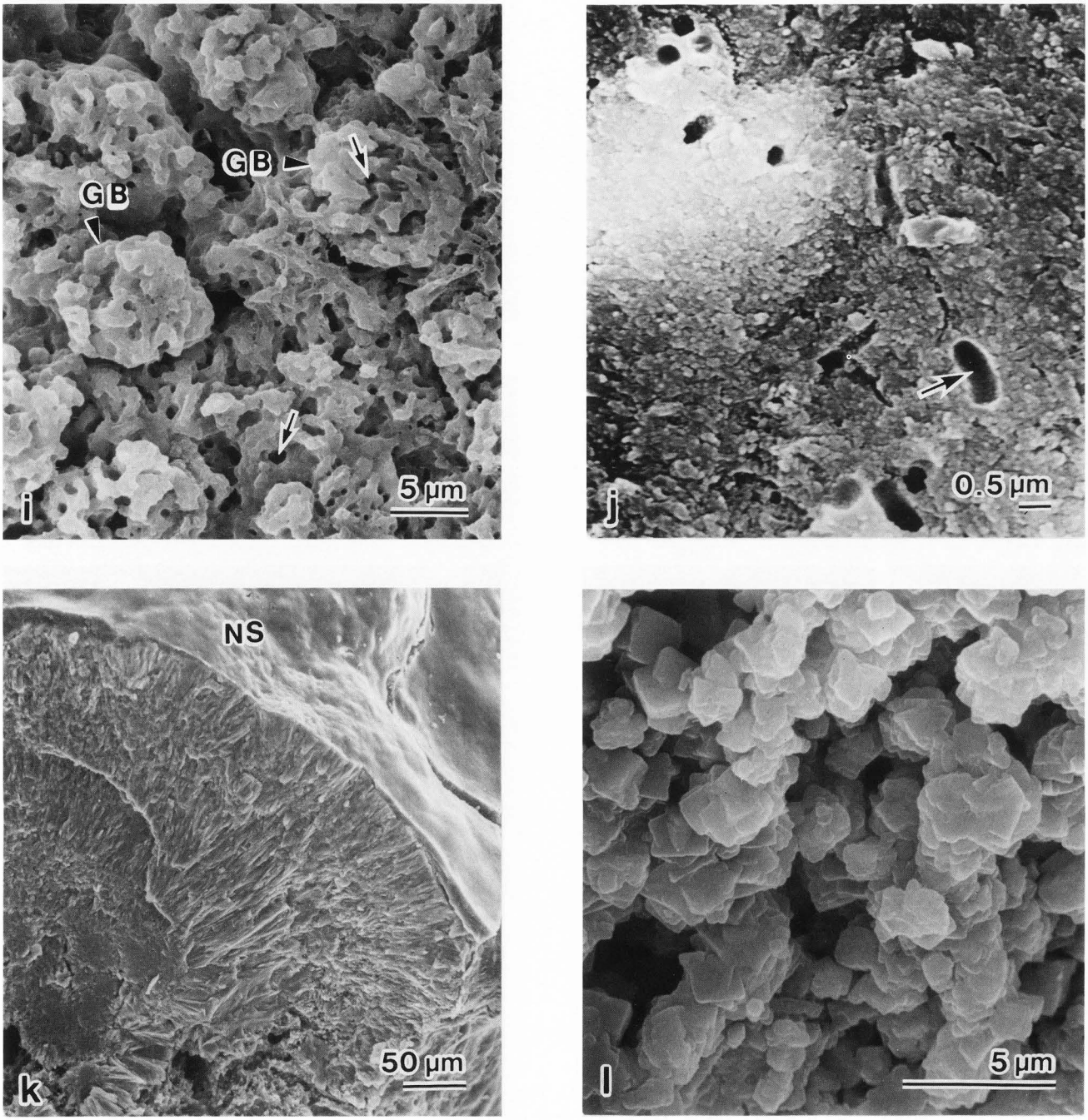

Figures 4i-4l: see page 250 for legends.

reported. We showed AP, OCP, and Mg-containing WH in accordance with the results by Burstein *et al.* [10]. Uroliths contained calcium phosphate crystals such as: AP [39, 67, 94]; DCPD [76]; AP and DCPD [16, 44, 78]; AP, DCPD, and WH [43]; and AP, DCPD, OCP, and WH [88]. We suggested AP with magnesium phosphates [16, 39, 43, 88] including struvite [78, 94] or Mg-containing AP, and showed OCP, and Mg-containing WH, but no DCPD was found. In rhinoliths, HAP or AP [1, 15, 75]; and WH [77] were reported, while we detected both AP and Mg-containing WH. In a tonsillolith, AP and HAP were reported [17], but we found OCP and Mg-containing WH as well as AP.

According to Schroeder's studies of human dental calculus [85, 86] and our previous SEM and EDX data [48, 53, 57], DCPD was characteristic in early calculus, while WH or Mg-containing WH appeared in older than young calculus. From the absence of DCPD and the

presence of WH, and their stone sizes (Figs. 1a-4a), all the samples in this study must be old stones. In dental calculus, WH crystals were not formed on the surfaces exposed to saliva [52, 53, 55, 71], although the crystals were formed on the subgingival calculus exposed to body fluid [53, 55]. The formation sites were the crevices of the tufts and lamellae of sound enamel in human old teeth [47], and in the subjacent dentinal tubules of attrited [56, 92, 93] and caries-arrested dentin [18]. In our SE-SEM observations of these stones, no WH crystals were found on their free surfaces.

Based on the later formation stages and sites of WH crystals in dental calculus and in human teeth, we suggest that the initial deposition of minerals in the rhinolith began from the periphery of the glomerulus-like nucleus of cotton strings by intra- and extracellular calcifications (Fig. 3c). After the nucleus was entirely sealed with the cortex of AP deposits, WH crystals were precipitated among the tubular strings, and on the outer surfaces and in the lumens (Figs. 3d-3h). Finally, the strings were replaced by WH deposits (Fig. 3f), similar to oral microorganisms in dental calculus [53] and collagen fibers in the subjacent dentinal tubules of attrited dentin [56].

We could not clarify the formation pattern of the tonsillolith; however, the formation might occur as follows. First, the conglomerates with microorganisms as the initial nuclei are formed mainly by the extracellular calcification in the degenerated palatine tonsil (Figs. 4d, 4h-4j), while in some internal areas, the conglomerates are semi-concentrically arranged (Fig. 4g). Secondly, the rhythmical deposition occurs around these initial nuclei by the extracellular calcification (Figs. 4c, 4e, and 4f). At almost the same time, AP and OCP deposition forms a rough cortex surrounding the interior (Figs. 4b, 4j, and 4k). Finally, WH crystals are precipitated in the internal spaces of the stone (Fig. 4l).

Acknowledgments

We are grateful to Dr. S. Eguchi and Dr. T. Ajiri who supplied valuable samples to us.

References

1. Abdel-Latif SM, Abdel-Hady S, Moustafa HM (1979). Crystallographic study of rhinolith. J Laryngol Otol **93**: 1205-1209.

2. Anneroth G, Eneroth CM, Isacsson G (1975). Morphology of salivary calculi. J Oral Pathol **4**: 257-265.

3. Anneroth G, Eneroth CM, Isacsson G (1975). Crystalline structure of salivary calculi. J Oral Pathol **4**: 266-272.

4. Appleton S, Kimbrough RE, Engstrom HIM (1988). Rhinolithiasis: a review. Oral Surg **65**: 693-698.

5. Barone JP, Nancollas GH (1978). The growth of calcium phosphates on hydroxyapatite crystals; the effect of fluoride and phosphonate. J Dent Res **57**: 735-742.

6. Beevers CA (1958). The crystal structure of dicalcium phosphate dihydrate, $CaHPO_4$-$2H_2O$. Acta Cryst **11**: 273-277.

7. Blatt IM, Denning RM, Zumberge JH, Maxwell JH (1958). Studies in sialolithiasis. Ann Otol Rhinol Laryngol **67**: 595-617.

8. Boyde A, Jones SJ (1983). Backscattered electron imaging of dental tissues. Anat Embryol **168**: 211-226.

9. Brown WE, Smith JP, Lehr JR, Fraxier AW (1962). Octacalcium phosphate and hydroxyapatite. Nature **196**: 1048-1055.

10. Burstein LS, Boskey AL, Tannenbaum PJ, Ponser AS, Mandel ID (1979). The crystal chemistry of submandibular and parotid salivary gland stones. J Oral Pathol **8**: 284-291.

11. Calvo C, Gopal R (1975). The crystal structure of whitlockite from the Palermo quarry. Am Mineral **60**: 120-133.

12. Castellano M, Marcolli G (1966). Calcolo tonsillare gigante simulante una neoplasia (Giant calculi of the tonsil simulating a neoplasm). Minerva Med **57**: 1686-1688 (in Italian).

13. Cheng P-T (1985). Octacalcium phosphate in vitro; implication for bone formation. Calcif Tissue Int **37**: 91-94.

14. Cheng P-T, Grabher JJ, LeGeros RZ (1988). Effects of magnesium on calcium phosphate formation. Magnesium **7**: 123-132.

15. Cheng P-T, Pritzker KPH, Richards J, Holymyad D (1987). Fictitious and human calculi with foreign nuclei. Scanning Microsc **1**: 2025-2302.

16. Cifuentes JM, Pourmand G (1980). Mineral composition of 103 stones from Iran. Brit J Urol **55**: 465-468.

17. Cooper MM, Steinberg JJ, Lastra M, Antopols S (1983). Tonsillar calculi: report of a case and review of the literature. Oral Surg **55**: 239-243.

18. Daculsi G, LeGeros RZ, Jean A, Kerebel B (1987). Possible physicochemical processes in human dentin caries. J Dent Res **66**: 1356-1359.

19. Driessens FCM (1982). Mineral aspect of dentistry. In: Monographs in Oral Science, Vol 10. Myers HM (ed.). Karger, Basel. pp. 1-215.

20. Eanes ED, Rattner SL (1981). The effect of magnesium on apatite formation in seeded supersaturated solutions at pH 7.4. J Dent Res **60**: 1719-1723.

21. Elidan J, Brama I, Gay J (1980). A large tonsillolith simulating tumor of the tonsil. Ear Nose Throat J **59**: 296-297.

22. Ennever J, Creamer H (1967). Microbiological

calcification, bone mineral and bacteria. Calcif Tissue Res **1**: 87-93.

23. Faure J, Vignoles M, Bonel G, Lodter JPh (1986). Microanalyse des calculs salivaires (Microanalysis of salivary calculus). J Biol Buccale **14**: 195-205 (in French).

24. Fichelson S, Tran CP, Frediere T, Laudenbach P (1978). Etude radiocrystallographique de 46 calculs salivaires (X-ray crystallographic examination of 46 salivary calculus). Revue Stomatol **79**: 75-90 (in French).

25. Frondel C (1941). Whitlockite: a new calcium phosphate, $Ca_3(PO_4)$. Am Mineral **26**: 145-152.

26. Gonzales F, Sognnaes RF (1960). Electron microscopy of dental calculus. Science **131**: 156-158.

27. Gonzalez-Diaz PF, Garcia-Ramos JV, Santos M (1979). Composition of apatites in human urinary calculi. Calcif Tissue Int **28**: 215-225.

28. Grøn P, Campen GJ, Lindstrom I (1976). Human dental calculus, inorganic chemical and crystallographic composition. Arch Oral Biol **12**: 829-837.

29. Hamad M, Heughebaert J-C (1986). The growth of whitlockite. J Crystal Growth **79**: 192-197.

30. Holma B, Granath L-E, Gustafson G (1970). A model for the study of tooth enamel by scanning electron microscopy. Odontol Rev **21**: 1-11.

31. Jensen AT, Danø M (1952). X-ray crystallographic examination of calculi from salivary glands. J Dent Res **31**: 620-626.

32. Jensen AT, Danø M (1954). Crystallography of dental calculus and the precipitation of certain calcium phosphate. J Dent Res. **33**: 741-750.

33. Jensen AT, Rowles SL (1967). Magnesium whitlockite, a major constituent of dental calculus. Acta Odontol Scand **16**: 121-139.

34. Jones SJ (1988). The root surface; an illustrated review of some scanning electron microscope studies. Scanning Microsc. **1**: 131-138.

35. Kani T, Kani M, Moriwaki T, Doi Y (1983). Microbeam X-ray diffraction analysis of dental calculus. J Dent Res **62**: 92-95.

36. Kaumann HS, Lillemore KD, Magnuson TH, Frasca P, Pitt HA (1990). Backscattered electron imaging and windowless energy dispersive X-ray microanalysis: a new technique for gallstone analysis. Scanning Microsc **4**: 853-862.

37. Kay MJ, Young RA, Posner AS (1964). Crystal structure of hydroxyapatite. Nature **204**: 1050-1052.

38. Keppler U (1965). Zum Whitlockit-Problem (On the whitlockite problem). Neues Jahrb Mineral Monatschr **6**: 171-176 (in German).

39. Khan SR, Hackett RL (1986). Identification of urinary stone and sediment crystals by scanning electron microscopy and X-ray microanalysis. J Urol **135**: 818-825.

40. Kahn SR, Wilkinson EJ (1985). Scanning electron microscopy, X-ray diffraction, and electron microprobe analysis on calcific deposits on intrauterine contraceptive devices. Human Pathol **16**: 732-738.

41. Khan SR, Wilkinson EJ (1990). Bladder stone in a human female: the case of an abnormally located intrauterine contraceptive device. Scanning Microsc **4**: 395-398.

42. Kim KM (1982). The stones. Scanning Electron Microsc **1982**; IV: 1635-1660.

43. Kim KM, Alpaugh HB, Johansen FB (1985). X-ray microanalysis of urinary stones; a comparison with other methods. Scanning Electron Microsc **1985**; III: 1239-1246.

44. Kim KM, Resau J, Chung J (1984). Scanning electron microscopy of urinary stone as a diagnostic tool. Scanning Electron Microsc. **1984**; IV: 1819-1831.

45. Knuuttila M, Lappalalinen R, Kontturi-Narhi V (1980). Effect of Zn and Mg on the formation of whitlockite in human subgingival calculus. Scand J Dent Res **88**: 513-516.

46. Kodaka T (1984). SEM images and XMA analysis of hard tissue treated with NaOCl. Acta Anat Nippon **59**: 486 (Abstract) (in Japanese).

47. Kodaka T, Debari K, Abe M (1992). Hexahedrally based crystals in human tooth enamel. Caries Res **26**: 69-76.

48. Kodaka T, Debari K, Higashi S (1988). Magnesium-containing crystals in human dental calculus. J Electron Microsc **37**: 73-80.

49. Kodaka T, Debari K, Mori R (1992). Backscattered electron microscopy of surface 'prismless' enamel in human permanent teeth. J Showa Univ Dent Soc **12**: 17-21.

50. Kodaka T, Debari K, Mori R (1992). SEM and XMA studies of human brain sands. J Electron Microsc **41**: 286 (Abstract).

51. Kodaka T, Debari K, Yamada M (1991). Physico-chemical and morphological studies of horse dentin. J Electron Microsc **40**: 385-391.

52. Kodaka T, Debari K, Yamada M (1991). Heterogeneity of crystals attached to the human enamel and cementum after calculus removal in vitro. Scanning Microsc **5**: 713-721.

53. Kodaka T, Hirayama A, Miake K, Higashi S (1989). Bacillus-shaped deposits composed of hexahedrally based crystals in human dental calculus. Scanning Microsc **3**: 843-854.

54. Kodaka T, Ishida I (1984). Observations of plate-like crystals in human dental calculus. Bull Tokyo Dent Coll **25**: 131-138.

55. Kodaka T, Miake K (1991). Inorganic components and the fine structures of marginal and deep subgingival calculus. Bull Tokyo Dent Coll **32**: 99-110.

56. Kodaka T, Nakajima F (1993). Rod-shaped deposits composed of whitlockite crystals in the dentinal tubules of attrited dentin. J Showa Univ Dent Soc **13**: 230-232.

57. Kodaka T, Ohohara Y, Debari K (1992). Scanning electron microscopy and energy-dispersive X-ray microanalysis studies of early dental calculus on resin plates exposed to human oral cavities. Scanning Microsc **6**: 475-486.

58. Konjiki T, Sudo T, Kohyama N (1980). Mineralographic notes of apatite in urinary calculi. Calcif Tissue Int **30**: 101-107.

59. LeGeros RZ (1985). Preparation of octacalcium phosphate (OCP): a direct fast method. Calcif Tissue Int **37**: 194-197.

60. LeGeros RZ (1991). Calcium phosphates in oral biology and medicine. In: Monographs in Oral Science, Vol 15. Myers HM (ed.). Karger, Basel. pp. 1-201.

61. LeGeros RZ, Daculsi G, Kijkowska R, Kerebel B (1989). The effect of magnesium on the formation of apatites and whitlockites. In: Magnesium in Health and Disease, Itokawa Y, Durlach J (eds.). John Libbey & Co Ltd., London. pp. 11-19.

62. LeGeros RZ, Daculsi G, Orly I, Torres W (1989). Solution-mediated transformation of octacalcium phosphate (OCP) to apatite. Scanning Microsc **3**: 129-138.

63. LeGeros RZ, Kijikowska R, LeGeros JP (1984). Formation and transformation of octacalcium phosphate, OCP: a preliminary report. Scanning Electron Microsc **1984**; IV: 1771-1777.

64. LeGeros RZ, Lee D, Quirolgico G, Shirra WP, Reish L (1983). In vitro formation of dicalcium phosphate dihydrate, $CaHPO_4$-$2H_2O$ (DCPD). Scanning Electron Microsc **1983**; I: 407-418.

65. LeGeros RZ, LeGeros JP (1972). Brushite crystals grown by diffusion in silica gel and in solution. J Crystal Growth **13**: 476-480.

66. LeGeros RZ, Orly I, LeGeros JP, Gomez C, Kazimiroff J, Tarpley T, Kerebel B (1988). Scanning electron microscopy and electron probe microanalysis of the crystalline components of human and animal dental calculi. Scanning Microsc **2**: 345-356.

67. Leusmann DB (1983). Routine analysis of urinary calculi by scanning electron microscopy. Scanning Electron Microsc **1983**; I: 387-396.

68. Mishenkin NV, Shtil AL (1965). Tonsillar calculi and the causes of their formation. Vestn Otorinolaringol **2**: 110-112 (in Russian).

69. Mishima H, Yamamoto H, Sakae T (1992). Scanning electron microscopy - energy dispersive spectroscopy and X-ray diffraction analyses of human salivary stones. Scanning Microsc **6**: 487-494.

70. Moriwaki Y, Doi Y, Kani Y, Aoba T, Taskahashi J, Okazaki M (1983). Synthesis of enamel-like apatite at physiological temperature and pH using ion-selective membranes. In: Mechanisms of Tooth Enamel Formation. Suga S (ed.). Quintessence Pub., Tokyo. pp. 239-256.

71. Nakagawa T (1983). Morphological study of unsusceptible occlusal pits and fissures against dental caries in old premolars. Jpn J Oral Biol **25**: 481-502 (in Japanese).

72. Newesely H (1965). Über die Existenzbedingungen von Octacalciumphosphat, Whitlockit und Carbonatapatit (On the formative conditions of octacalcium phosphate, whitlockite and carbonate apatite). Dtsch Zahnärztl Z. **20**: 753-766 (in German).

73. Okazaki M, Takahasi J, Kimura H (1986). Unstable behavior of magnesium-containing hydroxyapatites. Caries Res **20**: 324-331.

74. Pak CYC (1981). Potential etiologic role of brushite in the formation of calcium (renal) stones. J Crystal Growth **53**: 202-208.

75. Poll A, Wosiewitz U, Witting C (1987). Spontaner intra-antraler Rhinolith (Spontaneous intra-antral rhinolith). HNO **35**: 515-518 (in German).

76. Rasinger GA, Braundsütter F, Auinger A (1985). Rhinolithiasis - unter spezieller Berücksichtigung der Mineralogie (Rhinolitiasis - a special mineralogical consideration). HNO **33**: 65-69 (in German).

77. Rizzo AA, Martin GR, Scott DB, Mergenhagen SE (1962). Mineralization of bacteria. Science **135**: 439-441.

78. Rodgers AL (1985). The application of physicochemical procedures in the analysis of urinary calculi. Scanning Electron Microsc **1985**; II: 745-758.

79. Rodgers AL, Spector M (1986). Pancreatic calculi containing brushite: ultrastructure and pathogenesis. Calcif Tissue Int **39**: 342-347.

80. Rowles SL (1964). Biophysical studies on dental calculus in relation to periodontal disease. Dent Practit **5**: 2-7.

81. Ruzicka F (1984). Structure of sub- and supragingival dental calculus in human periodontics: an electron microscopic study. J Periodontal Res **19**: 317-327.

82. Sakae T, Yamamoto H, Hirai G (1981). Mode of occurrence of brushite and whitlockite in a sialolith. J Dent Res **60**: 842-844.

83. Santos M, Gonzalez-Diaz PF (1980). Ultrastructural study of apatites in human urinary calculi. Calcif Tissue Int **31**: 93-108.

84. Saxton CA (1968). Identification of octacalcium phosphate in human dental calculus by electron diffraction. Arch Oral Biol **13**: 243-246.

85. Schroeder HE (1969). Formation and Inhibition of Dental Calculus. Hans Huber, Berne. pp. 1-201.

86. Schroeder HE, Bambauer HU (1966). Stages of

calcium phosphate crystallization during calculus formation. Arch Oral Biol **11**: 1-14.

87. Sidaway DA (1980). A microbiological study of dental calculus, IV: an electron microscopic study of in vitro calcified microorganisms. J Periodontal Res **15**: 240-254.

88. Sundberg M, Friskopp J (1985). Crystallography of subgingival human dental calculus. Scand J Dent Res **93**: 30-38.

89. Sutor DJ, Scheidt S (1968). Identification standards for human urinary calculus components, using crystallographic methods. Brit J Urol **40**: 22-28.

90. Takazoe I, Kurahashi Y, Takuma S (1963). Electron microscopy of intracellular mineralization by oral filamentous microorganisms in vitro. J Dent Res **42**: 681-685.

91. Terpstra RA, Driessens FCM (1986). Magnesium in tooth enamel and synthetic apatites. Calcif Tissue Int **39**: 348-354.

92. Tronstad L (1973). Scanning electron microscopy of attrited dentinal surfaces and subjacent dentin in human teeth. Scand J Dent Res **81**: 112-122.

93. Tronstad L, Langeland K (1971). Electron microscopy of human dentin exposed by attrition. Scand J Dent Res **79**: 160-2171.

94. Weirich W, Frohneberg D, Ackermann D, Alken P (1984). Praktische Erfahrungen mit der antegraden lokalen Chemolyse von Struvit/Apatit-, Harnsaure- und Zystinsteinen in der Niere (Practical investigation of struvite calculus, apatite ulinary calculus, and cystine calculus in the kidney by local chemical analysis). Urol A **23**: 95-98 (in German).

95. Wosiewitz U (1983). Scanning electron microscopy in gallstones research. Scanning Electron Microsc **1983**; I: 419-430.

Discussion with Reviewers

R.Z. ReGeros: Do you have any experimental evidence to support the presence of HA, $Ca_{10}(PO_4)_6(OH)_2$ in biological system? We find that all the biological apatites we have investigated are carbonate apatites containing varying amounts of carbonate and magnesium.
Authors: No, we have no evidence other than the SEM-EDX data. Certainly, biological apatites will be Ca-deficient or carbonate apatites, and we believe your previous data [60-63, 66]; however, previous investigators had often called biological apatites hydroxyapatite as reviewed in the **Introduction**.

R.Z. ReGeros: We believe that some of the calcium phosphate phases (OCP, β-TCMP, CO_3-AP) present in the 'mature' human dental calculi may have formed by the hydrolysis of DCPD which are observed in 'young' but not in 'mature' calculi. Do you agree? Do you think that calcium phosphate phases found in the other pathological calcifications form in a similar manner?
Authors: Yes, we think this is the case in dental calculus [48, 57, 97] and the stones used in this study, while calcareous concretions or brain sands in the pineal body may start at the calcified pinealocytes in apatite phases [50, 96, 98].

H. Mishima: Were other elements except Ca, P and Mg detected in human calculi by SEM-EDX?
Authors: We did not detect any trace elements except Mg in this EDX analysis. However, wavelength-dispersive (WDX) analysis might have detected Na, S, and other elements [50].

H. Mishima: I think that non-collagenous proteins may have some function in the initial formation of human calculi. Could you comment on that?
Authors: We think so, but we have not discussed this because we have not investigated such an organic substance in this study.

A.L. Rodgers: I am surprised that struvite was not present in the urolith, particularly since microorganisms and bacterial molds were detected. Was the patient suffering from a urinary tract infection? Can you suggest why struvite was not present in this stone?
Authors: First, this study was aimed at investigating the compositions of calcium phosphate crystals and their distributions. We did not show any struvite reported by you [78] and Weirich *et al.* [94]. Usually, a chemical formula such as $Mg(NH_4)PO_4$-$6H_2O$ cannot be identified by conventional SEM-EDX, because no nitrogen (N) is detected. On the other hand, the existence of magnesium phosphates with apatites was suggested; therefore, struvite may be co-existent with apatites in the urolith. Secondly, no records of the patient were retained, other than that the stone was from a Japanese male aged 66 years who died of non-urinary disease. He underwent routine anatomical dissection at the School of Medicine, Showa University.

A.L. Rodgers: Aetiological theories of human calculi (urinary, prostatic, salivary, biliary, pancreatic) all invoke the concept of an organic matrix in some or other form. Did you find any evidence in support of this in the calculi which you investigated in the present study?
Authors: No, we did not find any organic matrix in this study, but we agree that the problem is interesting.

A.L. Rodgers: X-ray diffraction analysis should be performed, if possible.
Authors: We analyzed hexahedral crystals in dental cal-

culus with electron-beam diffraction [53]. The aim of the present study was to investigate the composition of calcium phosphate crystals and their distribution patterns, although the identification by SEM-EDX may be less definitive than by electron beam and X-ray diffraction. When the distribution of calcium phosphate is investigated in small areas, X-ray diffraction may not be useful since its resolution is not good enough. On the other hand, we think that numerous reports using X-ray and electron beam diffraction (see **References**) support our previous EDX data.

K.M. Kim: The major weakness of the paper lies on the method of crystal identification. The Ca/P ratio has been known not to be a reliable method of crystal identification mainly for the following reasons. Biological crystals are seldom ideal. Intimate coexistence of crystals with different Ca/P ratios may affect the ratio of each of them. Angular relations of the crystal surfaces to the incidental and reflected beams can significantly alter the elemental ratio obtained by EDX. In view of the small number of stones analyzed, it would have been possible to isolate crystals of different habits and conclusively identify them by crystallography.

Authors: We agree with your comment. However, this study was aimed at investigating the composition of calcium phosphate crystals and their distribution patterns in several calculi. In addition, we believe that numerous reports by using X-ray and electron-beam diffractions (see **References**) fully support our SEM-EDX data. The areas of SEM-EDX analysis are smaller than those of X-ray diffraction, while wider and deeper than those of transmission electron microscopy (TEM)-EDX analysis. In our present and previous studies [47, 48, 53-55, 57], a mass which involved much the same crystals in shape and size was quantitatively analyzed with SEM-EDX. According to our previous study [53], the TEM-EDX and SEM-EDX data of whitlockite crystals identified with electron-beam diffraction in dental calculus were similar in the amounts of Ca, P, and Mg amounts, respectively. Therefore, we think that the three-dimensional structure of small biological crystals does not influence the SEM-EDX analysis.

S.R. Khan: I am not sure which role stone processing has played in the appearance of various types of crystals the authors have examined. Processing has involved fixation, rinsing in water, air drying, treatment with sodium hypochlorite and EDTA. Many of these may produce artifacts.

Authors: NaOCl treatment and chemical fixation did not change the shapes of calcium phosphate crystals although NaOCl removed organic substances on the surfaces [30, 34, 46, 48, 51-55, 57], while EDTA, naturally, etched the surfaces. The combined treatment of NaOCl and EDTA, on the other hand, made a strong relief to calcified tissues and calculi [46, 50]. Certainly, the appearance cannot show a natural structure, but the difference between organic-rich and mineral-rich structures will be remarkable. The effects may be similar to those of the BSE images.

S.R. Khan: Tomazic *et al.* (J Biomed Mat Res **27**: 217, 1993) have recently shown that treatment with sodium hypochlorite may even change the elemental composition of calcium phosphate crystals and may result in a higher Ca/P ratio.

Authors: We have reported that human cementum treated with NaOCl showed higher Ca and P amounts than the cementum treated without NaOCl, while there were no differences in human tooth enamel [46]. These results indicate that SEM-EDX analysis cannot detect the internal spaces removed with NaOCl among the crystals. In our present and previous studies [47, 48, 50-55, 57], the calcified samples were neither treated with NaOCl nor with EDTA when analyzed quantitatively with SEM-EDX.

Additional References

96. Galliani I, Frank F, Gobbi P, Giangaspero F, Falcieri E (1989). Histochemical and ultrastructural study of the human pineal gland in the course of aging. J Submicrosc Cytol Pathol **21**: 571-578.

97. Kodaka T, Ohara Y (1994). Scanning electron microscopic observations of epitaxial growth-like crystals in human early and old dental calculi. J Showa Univ Dent Soc **14**: 116-119.

98. Kristič R (1986). Pineal calcification, its mechanism and significance. J Neural Transm (Suppl) **21**: 415-432.